Wave- and Anemometer-Based Sea Surface Wind (WASWind) for Climate Change Analysis*

HIROKI TOKINAGA

International Pacific Research Center, SOEST, University of Hawaii at Manoa, Honolulu, Hawaii

SHANG-PING XIE

International Pacific Research Center, and Department of Meteorology, SOEST, University of Hawaii at Manoa, Honolulu, Hawaii

ABSTRACT

Ship-based measurements of sea surface wind speed display a spurious upward trend due to increases in anemometer height. To correct this bias, the authors constructed a new sea surface wind dataset from ship observations of wind speed and wind wave height archived in the International Comprehensive Ocean–Atmosphere Data Set (ICOADS). The Wave- and Anemometer-based Sea surface Wind (WASWind) dataset is available for wind velocity and scalar speed at monthly resolution on a 4° × 4° longitude–latitude grid from 1950 to 2008. It substantially reduces the upward trend in wind speed through height correction for anemometer-measured winds, rejection of spurious Beaufort winds, and use of estimated winds from wind wave height. The reduced global upward trend is smallest among the existing global datasets of in situ observations and comparable with those of reanalysis products. Despite the significant reduction of globally averaged wind speed trend, WASWind features rich spatial structures in trend pattern, making it a valuable dataset for studies of climate changes on regional scales. Not only does the combination of ship winds and wind wave height successfully reproduce major modes of seasonal-to-decadal variability; its trend patterns are also physically consistent with sea level pressure (SLP) measurements. WASWind is in close agreement with wind changes in satellite measurements by the Special Sensor Microwave Imagers (SSM/Is) for the recent two decades. The agreement in trend pattern with such independent observations illustrates the utility of WASWind for climate trend analysis. An application to the South Asian summer monsoon is presented.

1. Introduction

Sea surface wind trends are of great importance to study climate change. In model projections of the future climate, scalar wind speed change is a principal factor for spatial patterns of sea surface temperature (SST) warming (Xie et al. 2010a). For example, coupled ocean–atmosphere general circulation model simulations under global warming scenarios predict a weakening (strengthening) of the northeast (southeast) trade winds. This

asymmetric wind change acts to enhance (reduce) the SST warming in the northern (southern) subtropics over the Pacific through wind–evaporation–SST (WES) feedback (Xie and Philander 1994). The wind-induced changes in surface evaporation also affect the global hydrological cycle (Richter and Xie 2008), and changes in wind stress curl play a key role in forcing regional distributions of sea level rise (Timmermann et al. 2010). The zonal wind at the equator is an important element of the Bjerknes feedback. In the equatorial Pacific, Vecchi et al. (2006) show a tendency of reduced easterly trades based on sea level pressure (SLP) data, suggestive of a weakening of the Walker circulation. In the equatorial Indian Ocean, the zonal wind change remains highly uncertain (e.g., Du and Xie 2008; Han et al. 2010; Trenary and Han 2008; Zheng et al. 2010).

Ship-observed sea surface wind data are not suitable at this point for wind trend studies because they suffer from a spurious trend (Bunker 1980; Cardone et al. 1990;

Ramage 1987; Whysall et al. 1987). The global average of ship winds shows a gradual increase from 6.4 m s^{-1} in 1958 to 6.8 m s^{-1} in 1982, reaching 7.5 m s^{-1} in 2002 (Thomas et al. 2008), as the height of anemometer (HOA) and ratio of the anemometer-measured to Beaufort wind reports have increased (Cardone et al. 1990; Peterson and Hasse 1987). The upward trend represents an increase of 20% for the last half century—so large as to mask real changes in wind speed. No significant trend in surface wind has been observed at relatively homogeneous ocean weather stations in the North Pacific and North Atlantic (Isemer 1995), and the globally averaged SLP-derived wind (Ward and Hoskins 1996) support that the upward trend is artificial owing to changes in the practice of shipboard measurements.

For climate trend analyses, a consistent dataset is required for a long period. Using a dynamically consistent data assimilation system, reanalysis products provide homogeneous datasets for recent decades and are widely used for studies of low-frequency variability and climate trends. However, those reanalysis products tend to be affected by changes in observational data sources, especially satellite observations. For example, most reanalysis products suffer from a spurious increasing trend in precipitation as a result of instrumental changes in the satellite-based atmospheric sounder measuring air temperature and water vapor (Onogi et al. 2007). Such a spurious trend in precipitation may distort surface wind trends over some regions where precipitation is strongly coupled with surface wind convergence. Wu and Xie (2003) report that wind shifts in the 1970s are inconsistent between in situ observations and the U.S. National Centers for Environmental Prediction (NCEP)/National Center for Atmospheric Research (NCAR) reanalysis over the equatorial central and eastern Pacific.

Berry and Kent (2010, 2009) have recently constructed a global in situ dataset of adjusted sea surface wind as part of the National Oceanography Centre, Southampton (NOCS) v2.0 dataset, using the International Comprehensive Ocean–Atmosphere Data Set (ICOADS, previously called COADS) (Woodruff et al. 1987, 2010; Worley et al. 2005) together with ship metadata from World Meteorological Organization Publication Number 47 (Kent et al. 2007). Their adjustments for the in situ wind bias are 1) height correction with HOA for measured winds, 2) application of Beaufort equivalent scale of Lindau (Lindau 1995) following the Thomas et al. (2005) method, and 3) use of time-varying, scaling factors for the difference between visual and anemometer wind speeds. The height correction with HOA is the most effective in reducing the upward trend in measured wind (Thomas et al. 2005; Thomas et al. 2008). Use of the Beaufort equivalent scale of Lindau and time-varying

scaling factors helps further correct the bias of estimated winds. Even after these wind adjustments, however, a significant upward trend still remains in the global means of both measured and estimated winds (Fig. 5 in Berry and Kent 2010). In addition, NOCS v2.0 currently provides only scalar wind speed without vector wind components, and the data period from 1973 to 2006 is too short to analyze long-term climate trends.

Toward a wind dataset of long consistency, we consider the use of wind wave observations in ICOADS. Gulev and Grigorieva (2004, 2006) show that ship-observed wind wave heights in the North Pacific and North Atlantic are closely correlated with local wind variability on interannual and longer time scales. This wave–wind relationship results from the physics that wind wave height is proportional to surface wind stress, a principal based on which satellite microwave radiometer and scatterometer estimate sea surface winds from space. Visual observations of wave fields are available over the global oceans in historical ship records of ICOADS for at least the last half century. The advantage of using wind wave height is that the wave observations are less affected by changes in observational practice than measured wind, suggesting the potential for wind wave heights to represent long-term trends in sea surface wind.

The present study estimates sea surface wind speed from wind wave height, calibrating it with the height-corrected 10-m wind. We construct a new sea surface wind dataset using height-corrected measured winds, Lindau-adjusted visual winds, and wind wave height. Our wave-enhanced surface wind dataset not only reproduces seasonal-to-decadal climate variability but also significantly reduces the spurious upward trend in sea surface wind. The resultant surface wind trends are physically consistent with those in SLP-derived winds and satellite observations. We will illustrate its application for climate trend analysis, using an example from the Indian summer monsoon.

The rest of this paper is organized as follows. Section 2 introduces the data and method for constructing our new dataset. Section 3 examines the performance of the dataset for variability on seasonal-to-decadal time scales. Section 4 shows its long-term trend by comparison with the other independent datasets and presents an example of application for the Indian summer monsoon. Section 5 is a summary and discussion.

2. Data and method

This section describes problems in wind and wave observations by ships, and presents a method for how to adjust winds, calibrate wind wave heights, and construct a long-term consistent dataset for climate trend analysis.

a. WASWind

Our new dataset, the Wave- and Anemometer-based Sea surface Wind (WASWind), is constructed from individual ship reports of ICOADS release 2.5 (Woodruff et al. 2010), including preliminary reports on the real-time global telecommunications system (GTS) in 2008. ICOADS (previously called COADS) has been extensively used not only for data construction (e.g., Berry and Kent 2009; Smith and Reynolds 2003) but also for studies of climatology (e.g., Norris 1998; Tokinaga et al. 2005; Tokinaga et al. 2009) and climate variability (e.g., Deser and Blackmon 1993; Deser et al. 2004; Mantua et al. 1997; Tanimoto et al. 1993; Xie et al. 2010b). Our WASWind has a monthly $4° \times 4°$ latitude–longitude resolution and covers 59 years from 1950 to 2008. While recent satellite measurements are limited to the recent two decades, ship observations are available for a much longer period over the global oceans. One possible disadvantage is the coarse resolution of ship observations, but the monthly $4° \times 4°$ latitude–longitude resolution is enough to represent basin-scale climate variabilities on seasonal-to-decadal and longer time scales. The strategy for our dataset construction is to adjust ship-measured winds for known HOA, omit unadjustable winds, and replace them with wave-based wind estimates to depict physically consistent climate trends. A detailed method for each data source is described in the following subsections.

1) MEASURED WIND

In ICOADS, there are two main categories of ship-observed surface wind: measured and estimated winds (Fig. 1a). The former is instrumentally measured with anemometers, and the latter is "visually estimated" from sea conditions, known as the Beaufort equivalent scale. The upward trend results from multiple factors in both measured and estimated winds.

Measured wind reports appeared around 1950, but its percentage was not so large until 1962 (Fig. 1a). After 1963, measured wind reports gradually increased in number and comprise most wind reports since 1980. In measured winds, increasing HOA is the major factor contributing to the upward trend (e.g., Kent and Taylor 1997; Kutsuwada 1994, 2000). As the ship size has increased, a globally averaged HOA has risen from about 21 m in 1970 to about 32 m by 2002, with the largest increases in the early 1990s (Thomas et al. 2008). While the WMO regulation recommends that ship-observed wind should be reported at a height of 10 m, most ship winds have been measured above the 10-m reference height and are reported without any adjustments before 2002 (Kent et al. 2007). Because the wind increases
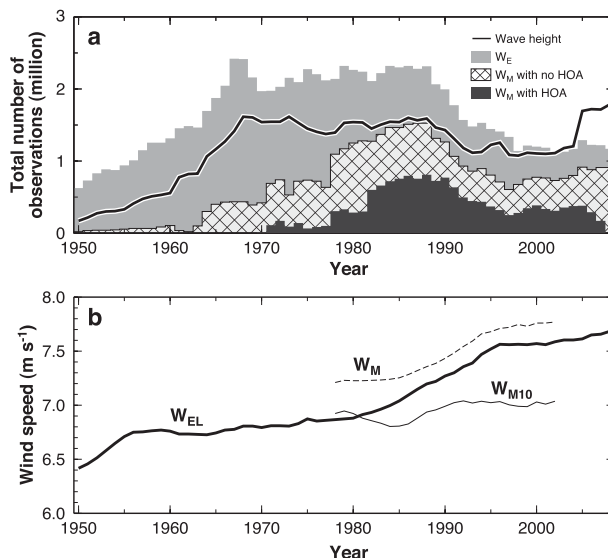

FIG. 1. (a) Time series of annual numbers of ship reports in ICOADS: Instrumentally measured wind with known (black bar) and unknown (cross-hatched bar) anemometer height, visually estimated wind (gray bar), and wind wave height (solid line). (b) Time series of annual averages of monthly mean wind speed (m s^{-1}): Lindau-adjusted estimated wind (W_{EL}, thick line), unadjusted measured wind (W_M, dashed line), and height-corrected 10-m measured wind (W_{M10}, thin line); W_M includes both measured winds with and without HOA.

with height in a typical vertical profile, the increase in HOA results in the spurious upward trend of the 10-m wind. In the present study, the height correction is applied only for the measured winds with known HOA, using a stability-dependent wind profile (Fairall et al. 2003). For the estimation of near-surface stability, SST, surface air temperature, and humidity in the same ship report are used. The height correction and elimination of wind reports with unknown HOA reduce the wind speed by 0.4–0.7 m s^{-1} and significantly remove the upward trend in unadjusted measured wind (Fig. 1b).

In WASWind, all measured winds with unknown HOA are omitted so as to reduce the spurious upward trend. This reduces data availability to about 50% of the total measured wind reports (Fig. 1a). NOCS v2.0 uses measured winds with unknown HOA using a height correction with a 2° gridded monthly averaged HOA dataset, which is a different approach from the present study. Since 2002, some ships began to use logging software, TurboWin, to process observations and adjust the observed wind speed to the 10-m reference height before transmission to GTS (Kent et al. 2007). Owing to limited metadata to determine which wind reports have been processed by TurboWin, this study does not analyze measured winds beyond 2002.

2) ESTIMATED WIND WITH THE BEAUFORT EQUIVALENT SCALE

We use the Beaufort equivalent wind scale of Lindau (1995) following the Thomas et al. (2005) method to adjust estimated winds. The visual wind estimate by the Beaufort equivalent scale was a mainstream of sea surface wind observations before the 1980s (Fig. 1a). After that, it gradually decreased in number but still accounts for 30% of total wind reports at present. Although the visually estimated winds should be unaffected by the spurious trend due to the HOA increase, they have a similar upward trend, especially after 1980 (Fig. 1b). Peterson and Hasse (1987) suggested that this upward trend is possibly because a large number of measured winds have been reported as estimated. This hypothesis is supported by a shift of the day − night difference after the 1980s. Thomas et al. (2008) suggest that nighttime visual wind observations tend to underestimate wind speed because of poor sight visibility for sea conditions. Comparing the daytime and nighttime estimated winds in ICOADS, they show that nighttime winds tend to be about 0.2–0.3 m s^{-1} lower than daytime winds before 1980. Since then, this diurnal difference got smaller as the number of measured wind reports rapidly increased. This characteristic of the day − night difference implies that a part of the estimated winds was actually measured by anemometers. Since it is difficult to indentify from ship metadata which reports were visually estimated, the present study omits the estimated winds after 1980. Figure 2a exhibits monthly averaged day − night differences in visually estimated wind for the period 1950–80. Except for data-sparse regions, the day − night differences are positive over most regions, and a similar tendency is also found in wind wave height (Fig. 2b). We use these monthly averaged day − night differences to correct nighttime observations for estimated wind and wind wave height.

3) WIND WAVE HEIGHT

Wind wave and swell observations are available in ICOADS for the whole period of our analysis. The height and period of wind waves and swell have been visually observed in 0.5-m increments and seconds, respectively. One possible uncertainty of visual wave observations is the separation between wind wave and swell. Gulev and Hasse (1999) examined the validity of the visual separation by comparing the wind wave and swell with wind speed over the North Atlantic. They found that wind waves are highly correlated with the local wind but swell is not, concluding that wind wave and swell are well separated in the COADS marine reports. In the present study, only wind wave heights with
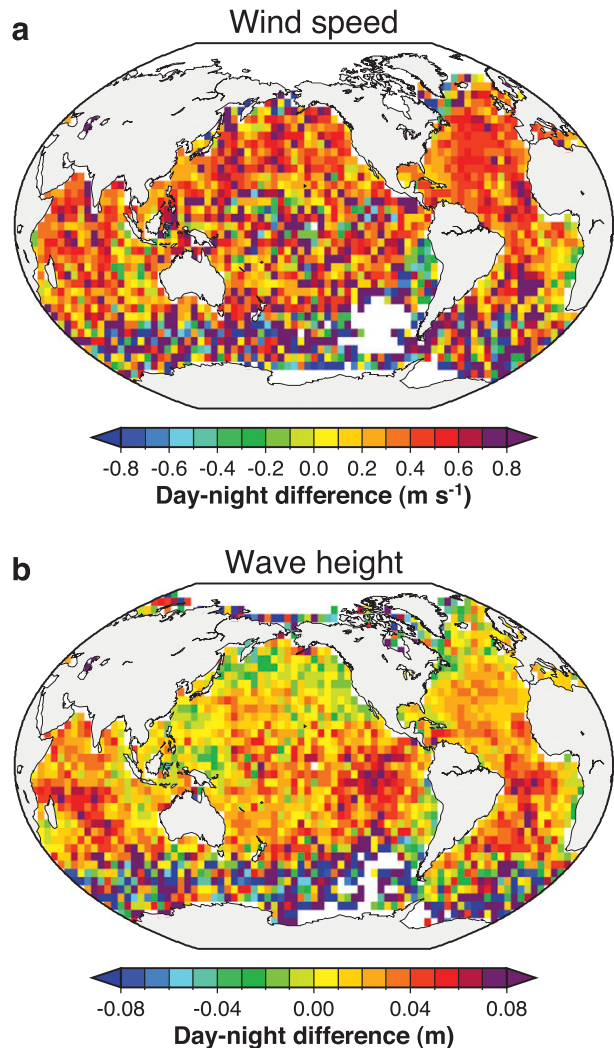
Wind speed

Day-night difference (m s^{-1})
-0.8 -0.6 -0.4 -0.2 0.0 0.2 0.4 0.6 0.8

Wave height

Day-night difference (m)
-0.08 -0.04 0.00 0.04 0.08

FIG. 2. Day − night differences of monthly-mean (a) visually estimated wind speed averaged for 1950–80 and (b) wind wave height for 1950–2008.

wave period less than 7 s are used to reject possible swells. Additionally, the wind wave observations are analyzed only for the two periods from 1950 to 1962 and 1969 to 2008 because of complicated changes in the reporting code around 1963 and 1968. Hereafter, wind wave is simply referred to as ''wave'' if not specified. Figure 3 summarizes how each data source is used in WASWind for different periods. For periods when the estimated and measured winds are omitted, wave observations fill the data gaps in wind reports (Fig. 1a).

To check whether wave height is a good alternative data source of sea surface wind, we first construct annual-mean climatologies of our quality-checked wave height and NOCS v2.0 10-m wind speed (Fig. 4). The wave height field features quite similar spatial patterns to those of the surface wind, with high waves in the midlatitude
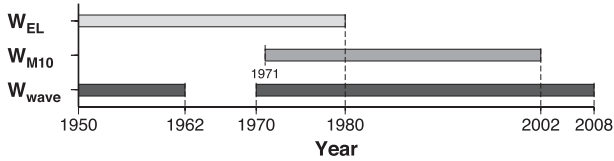
FIG. 3. Surface wind data sources (W_{EL}: Lindau-adjusted estimated wind, W_{M10}: height-corrected 10-m measured wind, and W_{wave}: wave height–estimated wind) analyzed in WASWind.

surface westerly and subtropical trade wind regions and low waves in the tropics and subtropical highs. The seasonal cycle of wave height captures the annual cycle of the midlatitude westerlies and trade winds over the Pacific and Atlantic, as well as the semiannual cycle of the Indian summer monsoon over the north Indian Ocean (Fig. 5). This covariability confirms the potential for using wave height to derive surface wind speed. While each wave height observation may include errors depending on observers, such random errors are reduced by averaging a large number of observations in a 4° grid box.

Wave heights are used to estimate the 10-m wind speed as follows. Figure 6 shows an example in a well-sampled grid box located in the North Atlantic. We first calculate a median value of the height-corrected 10-m wind in each wave height bin from simultaneously observed pairs of the two parameters (open circles in Fig. 6). Because the ship-observed surface wind sometimes includes unrealistic outliers, the use of a median value is necessary to reduce their effect. Based on the median values, a fitting curve function,

$$(\text{10-m wind speed}) = a(\text{wave height})^b + c,$$

is calculated by least squares method, where $a \geq 0$, $b \geq 0$, and $c \geq 0$ (thick curve in Fig. 6). In the grid box of Fig. 6, the coefficients a, b, and c are 6.2, 0.58, and 0.95, respectively. Overall, the coefficient a tends to take values of 5–7 (2–4) in the high (low) wind region, while the coefficient c is about 0–1.5 (2–3.5). The coefficient b takes relatively constant values of 0.5–0.7 over the global oceans, physically supporting that wave height is proportional to surface wind stress. Wind stress is also affected by ocean currents and atmospheric stability. Applying these coefficients, we can implicitly include effects of ocean currents and stability on wind stress. We construct a fitting curve for each calendar month and each grid box and use the same coefficients from 1950 to 2008. While this method does not take into account ocean current and stability changes on interannual and longer time scales, such effects are negligible compared with changes in surface wind. Zonal and meridional wind
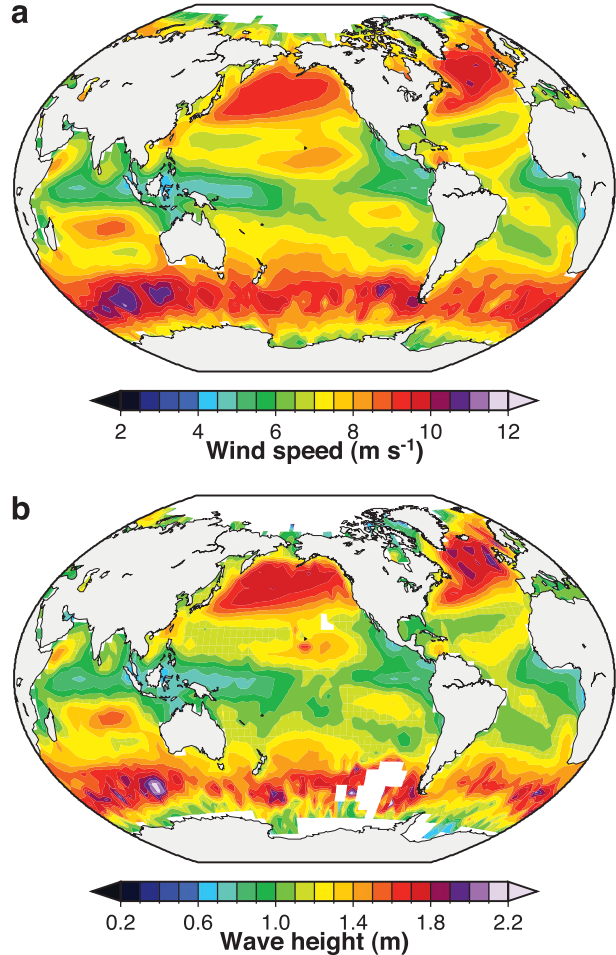

FIG. 4. Annual-mean climatology for 1973–2006: (a) NOCS v2.0 10-m wind speed (m s^{-1}) and (b) ICOADS wind wave height (m).

components are calculated from concurrent wind direction observations.

4) QUALITY CONTROL AND GRIDDING METHOD

ICOADS contains reports from ships and other in situ marine platforms such as moored and drifting buoys. In the present study, only ship data are analyzed. All data have been trimmed using a procedure that identifies potential outliers based on the climatological 3.5 standard deviation limits. This quality control is basically the same as that used for the standard product of the ICOADS Monthly Summary Groups (MSG). The same quality control is also applied for the wave-estimated 10-m winds.

To compare with standard products of the 2° × 2° ICOADS–MSG, we first construct an adjusted wind dataset on the same 2° × 2° grid by a box average. Next we regrid both datasets on a 4° × 4° grid, weighting the number of observations that contributed to each 2° × 2° monthly mean. In the present study, we use wave height
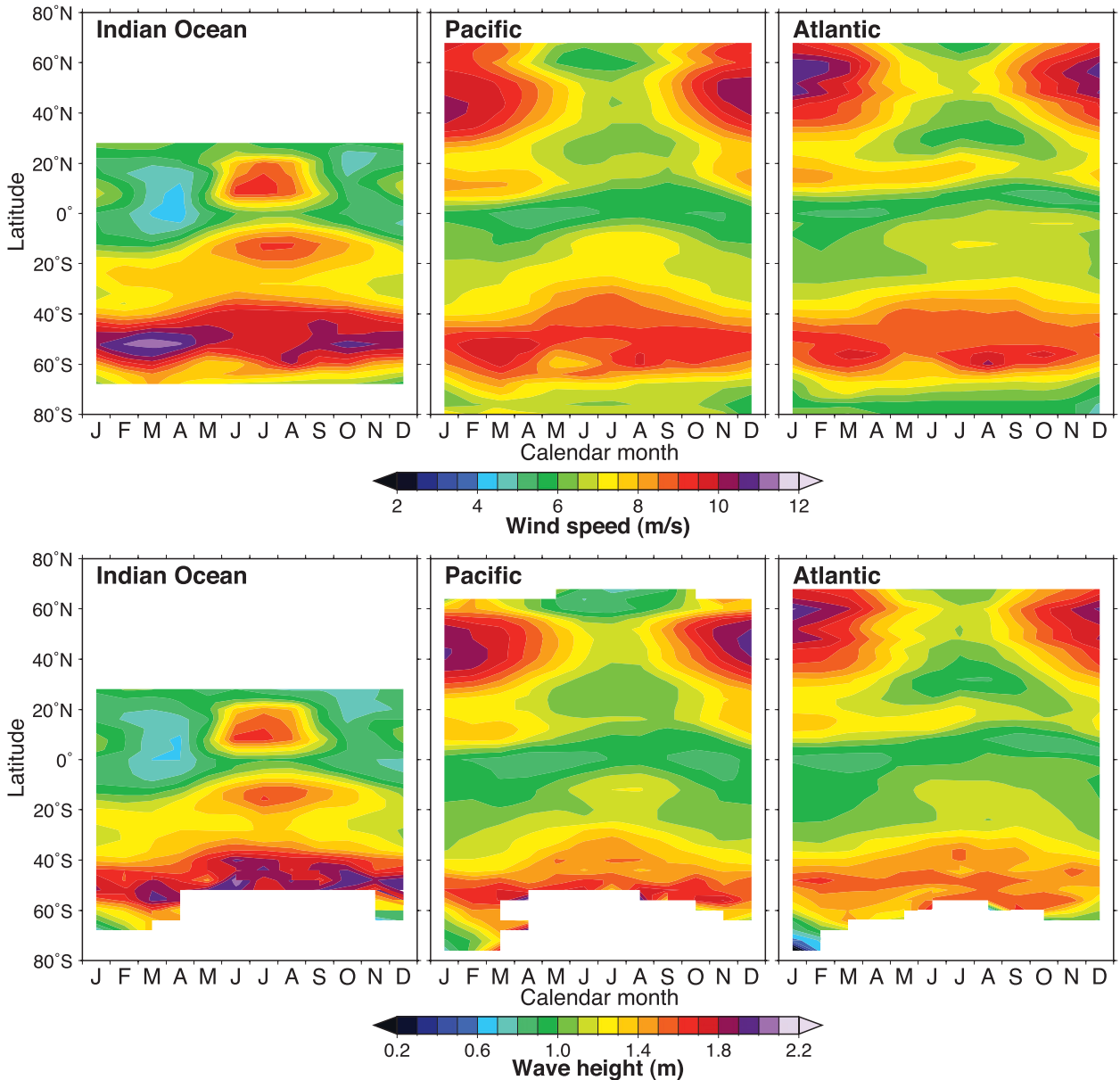
FIG. 5. (top) Zonally averaged climatological seasonal cycles of NOCS v2.0 10-m wind (m s^{-1}) and (bottom) ICOADS wind wave height (m) over the (left) Indian Ocean (30°–100°E), (middle) Pacific (120°E–100°W), and (right) Atlantic (70°W–20°E).

observations as an independent data source for wind speed. To increase sample numbers of wind data, we take a simple average of wave height estimated and measured (or Beaufort) winds when the two parameters are available in the same report. For visualization, we apply a weighted average using values at the grid point and eight surrounding points.

b. Data for comparison

To examine the performance of our newly constructed WASWind, we use a total of eight global surface wind products: three in situ, one satellite, and four reanalysis datasets. First, we regrid all datasets on the same 4° × 4° grid as WASWind. In the comparison of global-mean time series for all of the datasets and each calendar month, we use only well-sampled 4° grid boxes that contain observations for more than 75% of the total months so as to eliminate the effect of grid differences due to missing values in some datasets.

1) IN SITU OBSERVATIONS

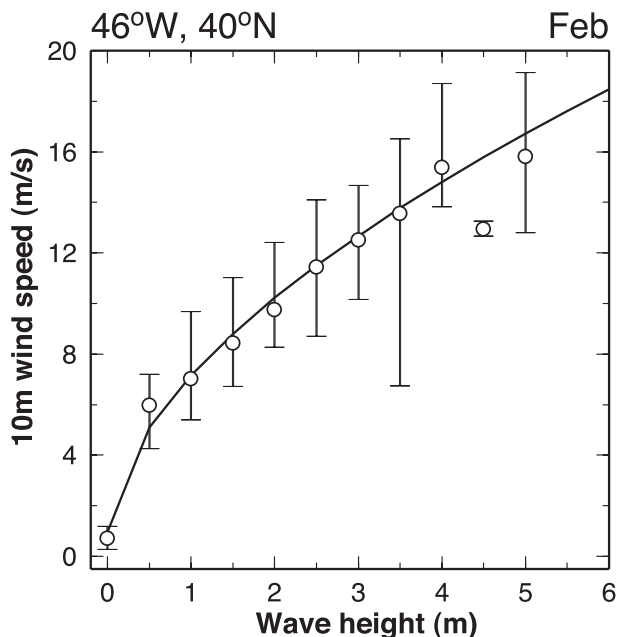Sea surface winds from the standard product of unadjusted ICOADS–MSG are available at monthly

FIG. 6. Relationship between wind wave height and 10-m wind speed in February on a well-sampled 4° grid box centered at 40°N, 46°W over the North Atlantic. The median value of 10-m wind speed in each wind wave height is shown by an open circle. The standard deviations (error bars) are calculated separately for below and over the median value. The thick line is a fitting curve function calculated by least squares method using all median values.

resolution for 1950–2008. Data source, period, gridding method, and quality control are basically the same between ICOADS–MSG and WASWind, except that WASWind is constructed with height-corrected winds, Lindau-adjusted estimated winds, and wave-estimated winds.

SLP from ICOADS is used as validation data. SLP is less affected by changes in observational practice than sea surface winds. Following the same method of Ward and Hoskins (1996), the balanced friction flow (BFF) field is constructed from a three-way balance of forces among SLP gradient, Coriolis, and friction. To fill gaps in data-sparse regions, SLP data are interpolated on a 10° grid using the Ward and Hoskin interpolation scheme. Using the same scheme, WASWind is also interpolated on the same 10° × 10° grid for comparison with the BFF field. The BFF data are available from 1950 to 2008. SST and cloud cover in ICOADS are also used to check physical consistency of wind variations in WASWind. To correct historical marine cloud cover records, we remove the tropical (30°N–30°S) mean cloud cover trend from each grid box following Deser and Phillips's (2006) method.

NOCS v2.0 has been constructed from the ICOADS release 2.4 (Berry and Kent 2010, 2009). This dataset is available at monthly resolution on a 1° × 1° grid for the period from 1973 to 2006. Optimal interpolation (OI) provides a dataset on the 1° grid with uncertainty estimates, although the effective spatial resolution is determined by the length scale of 300 km used in the OI. In NOCS v2.0, the visually estimated and anemometer-measured winds are separately adjusted. For the visual winds, Lindau's equivalent scale and empirical bias adjustments are applied. The empirical bias adjustment is conducted as follows. A factor of unit 1 prior to the end of 1985 that linearly decreases to 0.95 by 2000 is applied to visual wind speeds to bring the trends in the visual winds into agreement with those in height-corrected anemometer winds (Fig. 5 in Berry and Kent 2010). The anemometer winds are adjusted to the 10-m reference height using the wind profile of (Smith 1980, 1988) and known HOA. When HOAs are unknown, the defaults are based on a monthly 2° gridded dataset of HOA. This NOCS v2.0 approach analyzes maximum available visual and anemometer winds, whereas the present study uses only anemometer winds with known HOA and visual winds before 1980. Currently, the 10-m wind speed is available only for scalar but not vector winds in NOCS v2.0. The 10-m scalar wind field of NOCS v2.0 is regridded onto a 4° × 4° grid by a box average for the comparison with WASWind.

The University of Wisconsin—Milwaukee (UWM)/COADS is available at monthly resolution on a 1° grid from 1945 to 1993 (da Silva et al. 1994). The UWM–COADS adjusts visually estimated winds to the height of 20 m with their revised Beaufort equivalent scale, and it is assumed that all measured winds were obtained at the height of 20 m, which was an average of HOA during the analyzed period. Isemer and Hasse (1991) estimated that the 20-m wind speed is on average 7.5% larger than the 10-m wind speed.

2) SATELLITE OBSERVATIONS

The Special Sensor Microwave Imagers (SSM/Is) onboard the Defense Meteorological Satellite Program (DMSP) polar orbiting satellites have observed surface wind speed with a high spatiotemporal resolution over the global oceans since 1987 (Wentz 1997). A series of SSM/I observations are cross-calibrated between the DMSP satellites and validated by comparison with moored ocean buoys and satellite scatterometer wind retrievals at Remote Sensing Systems. Using the long record of SSM/I observations, Wentz et al. (2007) show that surface wind change has strongly affected the global hydrological cycle for the recent two decades. To compare their result and our trend analysis, we use the SSM/I surface wind speed for the same period from July 1987 to August 2006 and regrid the 0.25° × 0.25° dataset onto a 4° × 4° grid by a box

average. The data period is extended until 2008 for intercomparison of the global-mean time series with the other datasets.

3) REANALYSIS PRODUCTS

For the intercomparison of global-mean time series, we use four atmospheric reanalysis products from NCEP/NCAR (NRA1) (Kalnay et al. 1996) for 1950–2008, the NCEP–Department of Energy Reanalysis 2 (NRA2) (Kanamitsu et al. 2002) for 1979–2008, the European Centre for Medium-Range Weather Forecasting Reanalysis (ERA) (Uppala et al. 2005) for 1958–2001, and the Japanese Reanalysis (JRA) (Onogi et al. 2007) for 1979–2008. We first calculate monthly means of the 10-m scalar wind from 6-hourly data and regrid them into a $4° \times 4°$ grid. For the intercomparison of the global-mean time series, we exclude reanalysis data on the grid where an in situ or satellite datum is missing.

3. Seasonal-to-decadal variability

Before presenting a trend analysis, we examine major modes of seasonal-to-decadal variabilities in WASWind and evaluate its utility for climate variability study.

a. Seasonal cycle

Figure 7 compares seasonal cycles of 10-m wind speed in WASWind and SSM/I. WASWind shows very high correlations in the seasonal cycle with the SSM/I, exceeding +0.98 over most regions (Fig. 7a). The rms differences (RMSD) with the SSM/I wind are 0.3–0.6 m s^{-1} over the tropics and subtropics and 1–1.6 m s^{-1} over the extratropics (Fig. 7b). The large RMSD corresponds to high variability regions associated with storm tracks over the Kuroshio and Gulf Stream. In such regions, ship-observed winds tend to have a larger variance than the SSM/I owing to ship sampling errors. The large RMSDs are also found in the Southern Ocean possibly because of a reduction in observation number associated with the wind adjustments in the present study. Figure 7c shows a bias defined as the SSM/I minus WASWind. While the SSM/I estimates 10-m wind speed from surface roughness assuming neutral stability in the near-surface atmosphere, WASWind depends on atmospheric stability. Under stable (unstable) conditions, the 10-m neutral wind of satellite measurements tends to underestimate (overestimate) the actual 10-m wind (e.g., Liu et al. 2007). For example, the bias is about −0.5–0.7 m s^{-1} over the North Pacific and north Indian Ocean, with local maxima off the west coast of the Baja California peninsula, north of the Gulf Stream, the Kuril Islands northeast of Japan, the northwest Arabian Sea, and the equatorial eastern Pacific. These local maxima are regions of ocean upwelling
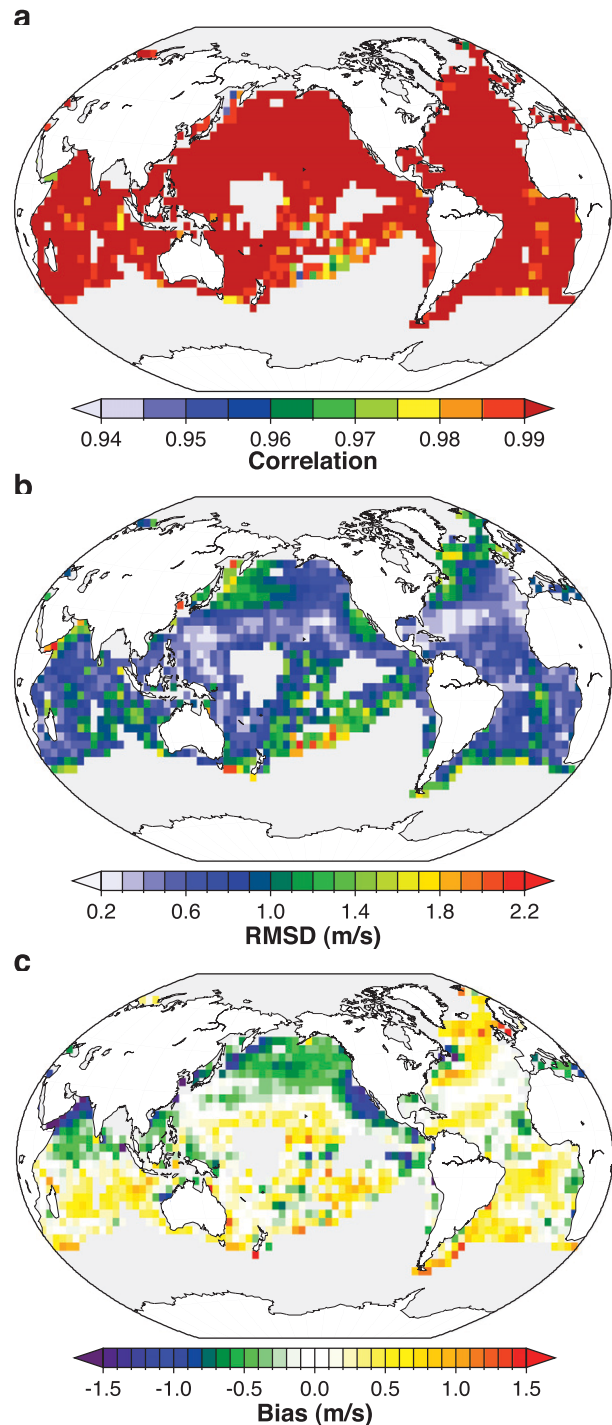

FIG. 7. Comparison of the WASWind monthly climatology with the SSM/I wind for 1988–2008: (a) Correlation coefficient, (b) RMSD (m s^{-1}), and (c) bias (m s^{-1}) defined as SSM/I minus WASWind.

or strong tidal mixing characterized by a stable near-surface atmosphere. By contrast, a local maximum of the positive bias is found on the warmer flank of the Gulf Stream where the near-surface atmosphere tends

to be unstable throughout the year, indicating an over-estimate by the SSM/I.

b. Interannual variability

The ENSO in the Pacific, Indian Ocean dipole (IOD), and Atlantic Niño are the major climate modes on interannual time scales. All of these climate modes are characterized by zonally asymmetric SST anomalies in the tropics that are closely coupled with equatorial zonal wind anomalies. The changes in SST are caused by anomalous equatorial zonal winds through changes in surface heat flux, upwelling, and oceanic Rossby and Kelvin waves. For this reason, the equatorial zonal wind indices have been extensively used to investigate the occurrence of ENSO (Wallace et al. 1998), IOD (Saji et al. 1999), and Atlantic Niño (Zebiak 1993) events. We construct the typical indices of SST and equatorial zonal wind anomalies from ICOADS and WASWind, respectively. To focus on interannual time scales, each time series is detrended and normalized by its standard deviation.

Figure 8a shows the November–January (NDJ) Niño-3.4 SST index and July–September (JAS) equatorial zonal-wind anomaly averaged within 4°S–4°N, 130°E–180°. El Niño in the eastern equatorial Pacific tends to occur in boreal winter and reaches its mature phase 3–4 months after the anomalous westerly wind anomalies in the western equatorial Pacific excite eastward-propagating equatorial downwelling Kelvin waves. The correlation coefficient between the Niño-3.4 and WASWind (ICOADS) equatorial zonal wind indices is +0.84 (+0.84), statistically significant at the 99% confidence level.

Similarly, Fig. 8b compares the September–November (SON) Dipole Mode Index (DMI) (Saji et al. 1999) and August–October equatorial zonal wind anomaly averaged within 4°S–4°N, 50°–70°E: note that the sign of DMI is reversed. The IOD is also a seasonally phase-locked interannual mode, often observed in boreal autumn, with a positive (negative) phase accompanied by anomalous equatorial surface easterlies (westerlies) over the central equatorial Indian Ocean (Saji et al. 1999; Webster et al. 1999). The correlation coefficient between DMI and WASWind (ICOADS) equatorial zonal wind indices is −0.85 (−0.83), statistically significant at the 99% confidence level. Specifically, the equatorial zonal wind index derived from WASWind successfully captures recent strong positive IOD events in 1994 and 1997 and a moderate positive event in 2006.

The Atlantic Niño is similar to El Niño in the equatorial Pacific except that it tends to take place in boreal summer. Figure 8c shows the June–August (JJA) Atlantic 3 SST index (ATL3; Zebiak 1993) and May–July equatorial zonal
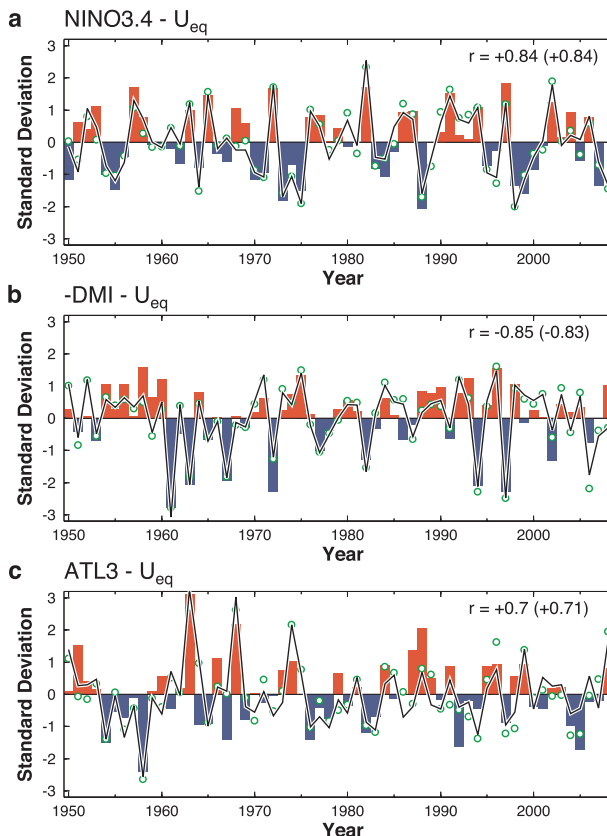

FIG. 8. Standardized time series of seasonally averaged SST indices (shaded bar) derived from ICOADS, and equatorial zonal wind anomaly indices (U_{eq}) derived from WASWind (solid line) and ICOADS (open circles): (a) NDJ Niño-3.4 index and JAS U_{eq} averaged over 130°E–180°, (b) negative SON DMI index and ASO U_{eq} averaged over 70°–90°E, and (c) JJA ATL3 index and MJJ U_{eq} averaged over 10°–40°W. All time series are detrended. Correlation coefficients between SST and WASWind (ICOADS–MSG) U_{eq} indices are shown at right top corner of each panel. All correlation coefficients are significant at 99% confidence level.

wind anomaly averaged within 4°S–4°N, 10°–40°W. Compared with the ENSO and IOD, the correlation coefficient between ATL3 and WASWind zonal wind indices is slightly lower ($r = +0.7$) but still significant at the 99% confidence level. This is not due to our reconstruction method; the unadjusted ICOADS shows a comparable correlation between ATL3 and zonal wind indices at $r = +0.71$.

Therefore, WASWind successfully reproduces high correlations in major climate modes between SST and equatorial zonal wind anomalies over the tropical Pacific, Indian Ocean, and Atlantic. Zonal SLP gradients across each ocean basin also significantly correlate with these equatorial zonal wind indices (not shown), further illustrating the ability of WASWind to capture interannual variability.
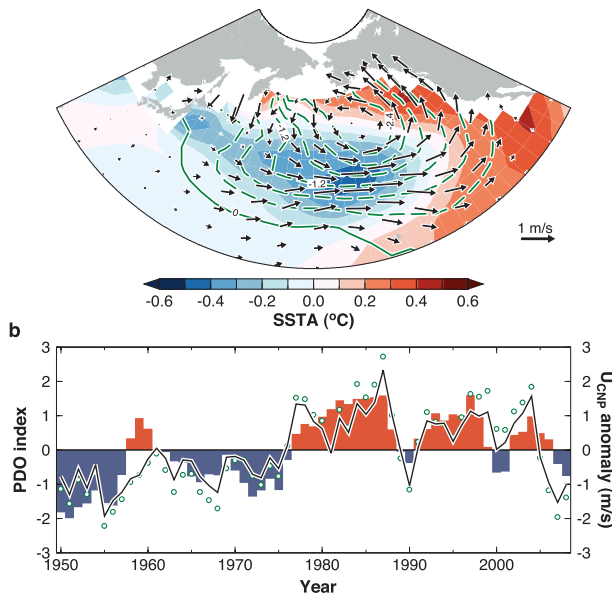
a Regression onto PDO index

b

a Regression onto NAO index

b

FIG. 9. (a) Regression coefficients of SST (color in °C), SLP (contours at 0.4 hPa intervals), and WASWind (vectors in m s^{-1}) with the PDO index for the JFM season. (b) Time series of the PDO index (shaded bar) and zonal wind anomaly averaged within 35°–40°N, 160°W–180° (WASWind: solid line and ICOADS: open circles) for the JFM season. The correlation coefficient between the PDO and WASWind (ICOADS) zonal wind indices is +0.78 (+0.78), significant at the 95% confidence level.
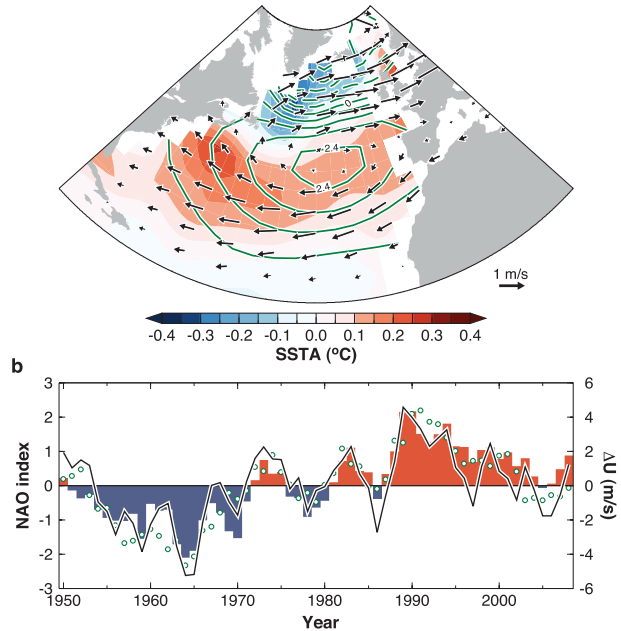
FIG. 10. (a) As in Fig. 10a but for regression coefficients with the NAO index and SLP contours at 0.6-hPa intervals. (b) Time series of the NAO index (shaded bar) and surface wind vorticity defined as (50°–60°N) minus (30°–40°N) zonal wind difference averaged between 10° and 40°W (WASWind: solid line and ICOADS: open circles) for JFM season. The correlation coefficient between the NAO and WASWind (ICOADS) vorticity indices is +0.85 (+0.92), significant at the 95% confidence level.

c. Decadal variability

WASWind also reproduces the surface wind pattern associated with the Pacific decadal oscillation (PDO) (Mantua et al. 1997). Figure 9a exhibits regression coefficients of the surface wind vector, SLP, and SST with the PDO index, defined as the leading principal component of the January–March mean SST anomalies in the North Pacific (20°–60°N, 120°E–110°W). The positive (negative) PDO, characterized by negative (positive) SST anomalies in the central North Pacific, takes place in years with a deepened (weakened) Aleutian low (Mantua et al. 1997). WASWind shows that surface winds are roughly in geostrophic balance with the deepened Aleutian low, with a local maximum of the surface westerly (easterly) anomaly over the negative (positive) SST anomalies in the central Pacific. Figure 9b shows time series of the PDO index and zonal wind anomaly averaged over the central Pacific (35°–40°N, 160°W–180°). The zonal wind index derived from WASWind shows an easterly (westerly) anomaly during the negative (positive) phase of PDO from 1950 to 1977 (from 1978 to 2006). While WASWind successfully captures the climate regime shift observed in 1976/77 (Hanawa et al. 1996; Mantua et al. 1997; Nakamura et al. 1997),

the decadal shift in WASWind zonal wind from 1966–75 to 1977–86 is 25% smaller than that in uncorrected ICOADS zonal wind. The correlation coefficient between the PDO and WASWind (ICOADS) zonal wind indices is +0.78 (+0.78), significant at the 95% confidence level.

The North Atlantic Oscillation (NAO) is the dominant mode of the atmosphere over the North Atlantic, characterized by a dipole SLP pattern between the Icelandic low and Azores high with a decadal fluctuation (Hurrell 1995; Hurrell and VanLoon 1997). Deser and Blackmon (1993) indicate that SST variability is coupled to surface wind variability associated with the NAO. Figure 10a shows regression coefficients of the surface wind vector, SLP, and SST with the NAO index defined by Barnston and Livezey (1987). WASWind is again in geostrophic balance with the NAO SLP pattern. As revealed by Deser and Blackmon (1993), the acceleration (deceleration) of climatological westerlies leads to negative (positive) SST anomalies north (south) of 40°N through enhanced (suppressed) upward surface heat flux and ocean mixing. The surface wind vorticity, defined as a meridional difference in zonal wind between (50°–60°N, 10°–40°W) and (30°–40°N, 10°–40°W), significantly correlates with
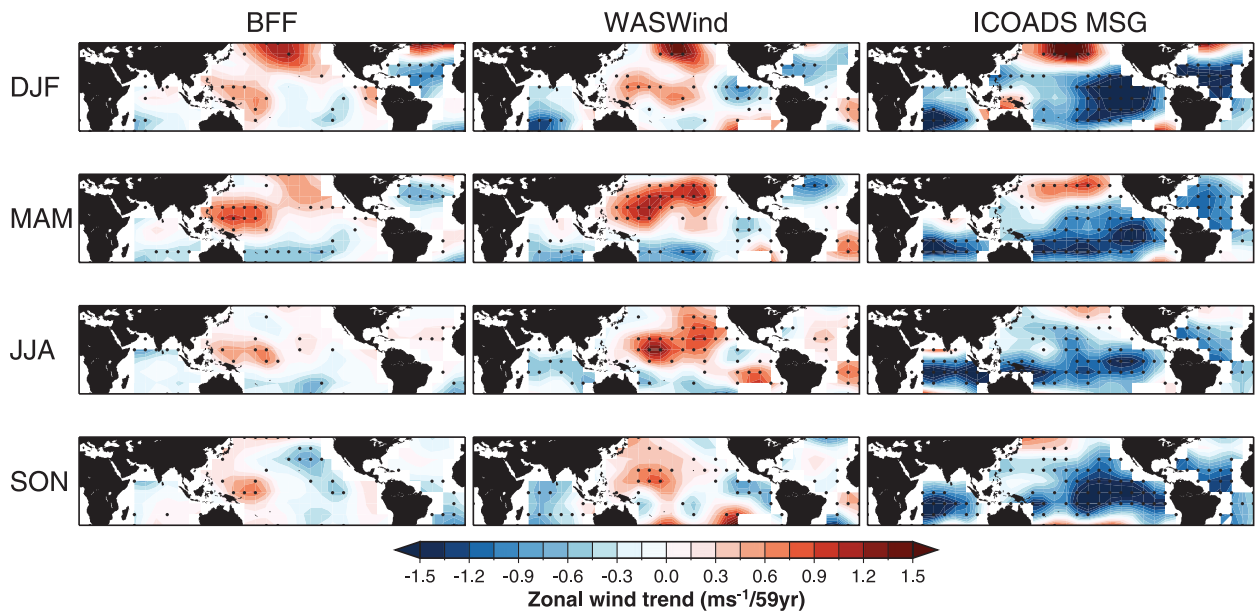
FIG. 11. Seasonally averaged linear trends in surface zonal wind for 1950–2008 derived from (left) BFF, (middle) WASWind, and (right) ICOADS–MSG. Grid points marked with dots exceed the 90% confidence level based on the Mann–Kendall test.

the NAO index ($r = +0.85$, significant at the 95% confidence level), consistent with intensification of the NAO during 1964–90 and weakening during 1950–64 and 1990–2006 (Fig. 10b).

4. Trends

Having established that WASWind well captures wind variability on seasonal-to-decadal time scales, we now examine secular trends. Specifically, we investigate to what extent the new dataset succeeds in removing the spurious trend in ship-based wind measurement in comparison with the unadjusted ICOADS–MSG winds, SLP-derived BFF winds, the SSM/I winds, and reanalysis products. Linear trends are calculated from least squares linear regression lines fitted to the data. The significance for the trends is estimated from the Mann–Kendall test.

a. Zonal and meridional wind trends

Figure 11 compares linear trends in zonal wind for 1950–2008 derived from SLP-derived BFF, WASWind, and ICOADS–MSG. BFF and WASWind exhibit westerly trends over the North Pacific during the December–February (DJF) and March–May (MAM) seasons and the western tropical Pacific throughout the year, which are consistent with deepening of the Aleutian low (Deser and Phillips 2009) and weakening of the trade winds (Clarke and Lebedev 1996), respectively. The seasonality

and regionality of the easterly trend in WASWind is also similar to those in BFF, especially over the south Indian Ocean, South Pacific, and subtropical North Atlantic. By contrast, the unadjusted ICOADS–MSG exhibits intensifications of the climatological zonal wind everywhere. For example, westerlies in the midlatitudes of the North Pacific and Atlantic, and trade winds in the tropics and subtropics, are intensified throughout the year. Such intensification of climatological wind appears to be due to the artificial upward trend in unadjusted wind. The spatial correlation, RMSD, and bias defined as the WASWind (ICOADS–MSG) minus BFF are summarized in Table 1. WASWind tends to show higher spatial correlations and lower RMSDs and biases than ICOADS–MSG throughout the year. The spatial correlations of WASWind with BFF appear to be not as high in the JJA and SON seasons (0.4 and 0.25, respectively), but its RMSDs and biases are significantly lower than for ICOADS–MSG.

BFF and WASWind also have a similar trend pattern in meridional wind between themselves (Fig. 12), yielding significant spatial correlation except for the SON season (Table 2). ICOADS–MSG appears to have a similar trend pattern to BFF and WASWind but shows stronger southerly trends off the west coasts of Australia, South America, and Africa, each of which corresponds to the regions of climatological southeasterly trade winds. RMSDs of WASWind are 0.1–0.2 m s^{-1} decade^{-1} lower than those of ICOADS–MSG, indicating an improvement due to the wind adjustment.

TABLE 1. Comparison of the WASWind and ICOADS–MSG dataset zonal wind trends with BFF. Bias is defined as WASWind (ICOADS–MSG) minus BFF trends. Significant correlations exceeding the 90% confidence level are emboldened. A two-tailed Student's t test is used for the significance test assuming that a degree of freedom is 14, estimated from numbers of regional patches showing positive and negative trends.

	Spatial correlation		RMSD (m s^{-1} decade^{-1})		Bias (m s^{-1} decade^{-1})	
Season	WASWind	ICOADS–MSG	WASWind	ICOADS–MSG	WASWind	ICOADS–MSG
DJF	**0.51**	**0.58**	0.50	0.91	−0.08	−0.62
MAM	**0.68**	**0.43**	0.40	0.46	0.01	−0.57
JJA	0.40	−0.11	0.45	0.89	0.14	−0.52
SON	0.25	0.21	0.47	0.83	0.05	−0.59

b. Scalar wind trend

Figure 13 shows scalar wind trends derived from WASWind and ICOADS–MSG for the period 1950–2008. As previous studies suggested, the unadjusted ICOADS–MSG exhibits positive trends in scalar wind speed all over the global oceans throughout the year. By contrast, the positive trends are significantly reduced in WASWind by the wind adjustments and use of wave height observations. WASWind shows negative trends in the subtropical North Pacific, south of Green Island, and the tropical South Atlantic. Negative trends in the subtropical North Pacific are most prominent in boreal spring and summer, associated with the reduction in the northeast trade winds observed in the vector wind fields (Figs. 11 and 12) and consistent with global warming simulations (Xie et al. 2010a). The WASWind is also consistent with the long-term positive (negative) trend in wintertime wind wave height over the North Pacific

(northeast Atlantic) revealed by Gulev and Grigorieva (2006).

To be precise, however, the scalar-mean wind speed is different from the magnitude of vector-mean wind. This difference arises from steadiness of the wind direction. While the vector-mean wind is useful to infer mean wind speed along its prevailing direction, the scalar-mean wind is the average strength of wind speed resulting not only from prevailing winds but also from weather disturbances. For example, the scalar and vector winds in WASWind show an opposite trend over the subtropical North Atlantic. While southwesterly trends in the vector wind field indicate a reduction in the climatological northeasterly trade wind in JJA and SON seasons, the scalar wind trend shows positive trends over the region. These opposite trends are possibly due to an intensification of tropical cyclone activity observed over recent decades (Elsner et al. 2008). Such synoptic cyclones with high winds can contribute to the increase in the
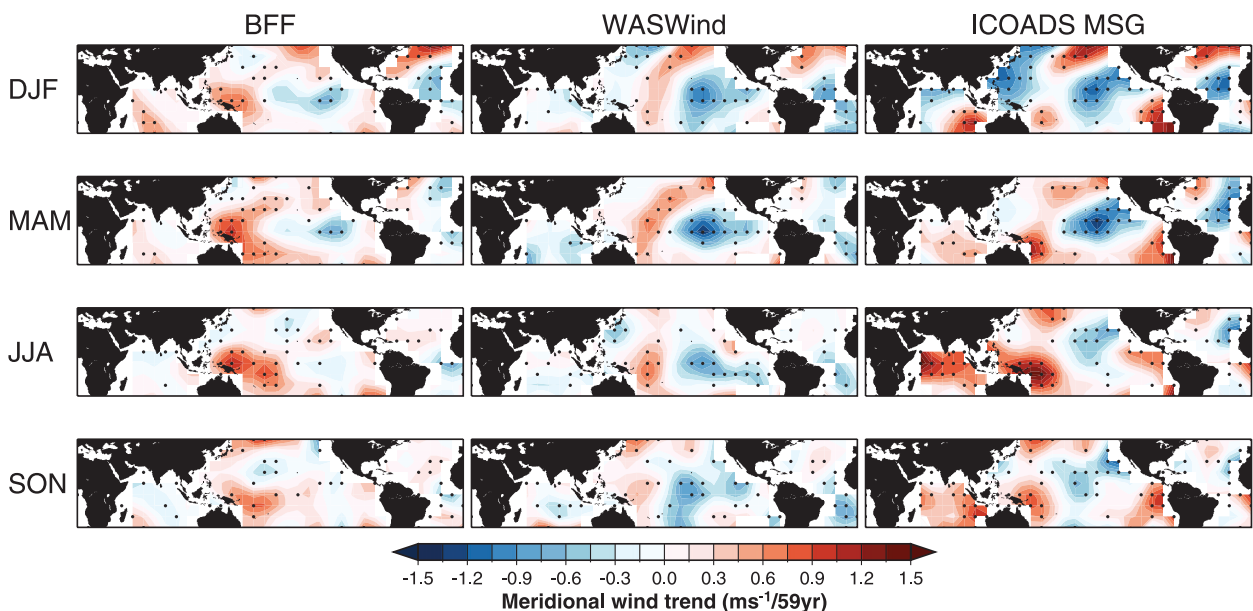

FIG. 12. As in Fig. 12 but for the surface meridional wind.

TABLE 2. As in Table 1 but for meridional wind trends.

Season	Spatial correlation		RMSD (m s⁻¹ decade⁻¹)		Bias (m s⁻¹ decade⁻¹)	
	WASWind	ICOADS–MSG	WASWind	ICOADS–MSG	WASWind	ICOADS–MSG
DJF	**0.62**	0.39	0.39	0.63	−0.21	−0.23
MAM	**0.58**	**0.43**	0.38	0.49	−0.18	−0.08
JJA	**0.44**	0.20	0.36	0.57	−0.16	0.15
SON	0.28	0.15	0.39	0.48	−0.17	0.04

scalar-mean wind but do not contribute much to the vector-mean wind.

Figure 14a compares a time series of the globally averaged annual scalar wind obtained from available in situ and satellite observations and reanalysis products. For the calculation of the global time series, we use only well-sampled 4° grid boxes that contain observations for more than 75% of the total months. Although a weak wind trend remains in WASWind, it is the smallest among the existing global datasets of in situ observations and comparable with that of the reanalysis products. The other two in situ datasets, UWM–COADS and NOCS v2.0, also reduce the upward trend, but their trends are still 0.1 m s⁻¹ decade⁻¹ larger than that of WASWind (Table 3). This difference is probably due to the correction methods used in each dataset. It may be not surprising that UWM–COADS has the larger upward trend since it adjusts only visually estimated winds, assuming that all measured winds were obtained at 20-m height. While both NOCS v2.0 and WASWind apply the height correction and use the same Beaufort wind scale, only WASWind has estimated 10-m winds from wave height observations and rejected all visually estimated winds reported after 1980. As a result, WASWind exhibits a smaller trend of +0.07 to +0.1 m s⁻¹ decade⁻¹.

Figure 14b shows the linear trend of the global-mean scalar wind speed and spatial standard deviation of the scalar wind trend pattern calculated from WASWind as a function of calendar month for the period 1950–2008. The global-mean trends are less than 0.1 m s⁻¹ decade⁻¹ throughout the year (dashed line in Fig. 14b). By contrast, the spatial standard deviations of trend pattern are more than 2.5 times as large, indicating that the surface wind trend has pronounced regional patterns.

Such rich regional trend patterns can be found in satellite-measured surface wind. As the longest satellite wind product, the SSM/I surface winds are now available for more than 20 years. The SSM/I observations have been cross-calibrated among a series of different DMSP satellites and validated by comparisons with moored ocean buoys and satellite scatterometer wind retrievals (Wentz et al. 2007). Recently, Wentz et al. presented the last 20-yr trend in SSM/I wind over the global oceans. Figure 15a is basically the same trend pattern as presented

in Wentz et al. (2007) except for grid size and map projection. The SSM/I captures a tripole structure over the North Atlantic associated with a recent decrease in the NAO after 1989 (Fig. 10b). The SSM/I also exhibits negative (positive) wind trends over the western Pacific and north Indian Ocean (the North Pacific, central tropical Pacific, and Southern Ocean). The global-mean time series shows an upward trend of +0.134 m s⁻¹ decade⁻¹ for the period 1988–2008 (Fig. 14a and Table 3).

WASWind features quite similar trend patterns to the SSM/I (Fig. 15b), capturing the tripole structure over the North Atlantic, the negative trends over the western Pacific and north Indian Ocean, and the positive trends over the central tropical Pacific and south Indian Ocean. NOCS v2.0 also captures the tripole pattern over the North Atlantic, but shows a broad positive trend pattern except for several patches of a negative trend over the Southern Ocean (Fig. 15c). Major differences exist in the tropical Indo–western Pacific Oceans from either SSM/I or WASWind. The spatial correlation coefficient, RMSD, and bias—defined as the WASWind (NOCS v2.0) minus SSM/I trends—are summarized in Table 4. For all of these statistics, WASWind shows better results than NOCS v2.0, especially as RMSD and the bias of WASWind trends are about 30% and 90% smaller than those of NOCS v2.0, respectively. This good agreement between WASWind and SSM/I wind trends suggests that visually observed wind wave heights are unlikely strongly affected by the increased ship size.

c. Indian summer monsoon

Previous studies of reanalysis products have suggested a weakening of the atmospheric circulation associated with the Indian summer monsoon from the Arabian Sea to South China Sea for recent decades, in response to a reduced thermal contrast between East Asia and the tropical Indian Ocean during boreal summer (Wu 2005). This weakening of the Indian summer monsoon is also apparent in rain gauge observations showing a significant decreasing trend over most subdivisions of India (Naidu et al. 2009). The attendant surface wind change has not been examined because of the spurious intensification of climatological winds in ship observations. With a weakened Indian summer monsoon, the
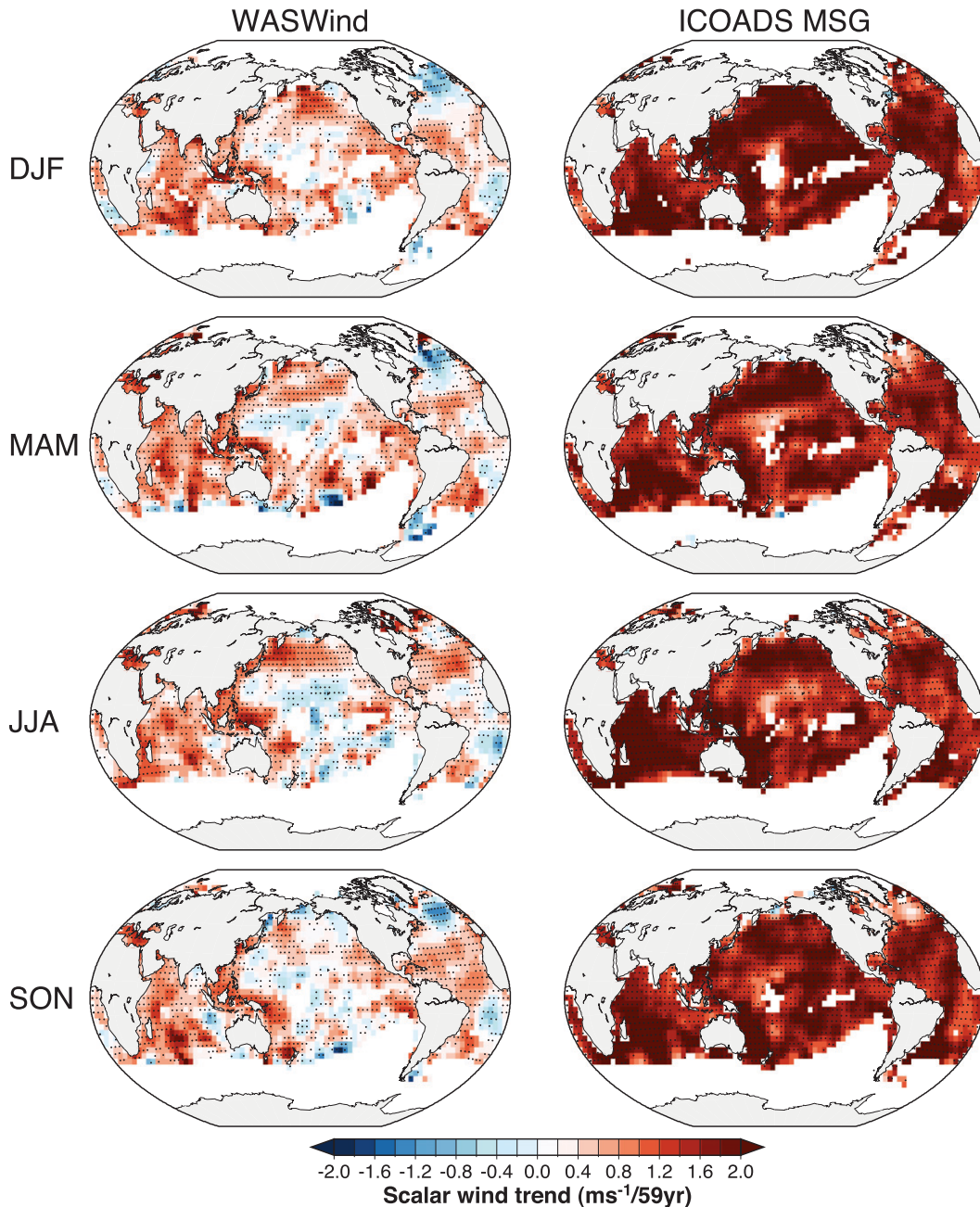
FIG. 13. Seasonally averaged linear trends in surface scalar-mean wind for 1950–2008 derived from (left) WASWind and (right) ICOADS–MSG. Grid points marked with dots exceed the 90% confidence level based on the Mann–Kendall test.

surface wind change is likely to oppose the climatological southwesterly wind, offering a good example to evaluate the performance of the wind adjustments used in WASWind.

Figure 16 exhibits climatologies and trends of the surface vector wind and cloud cover over the north Indian Ocean as a function of longitude and calendar month. Climatologically, the southwesterly-to-westerly

winds associated with the Indian summer monsoon start in June and persist until September, accompanied by increased cloud cover off the west coast of India and over the Bay of Bengal (Fig. 16a). While the unadjusted ICOADS–MSG has an increasing trend of the climatological southwesterly-to-westerly winds (black arrows in Fig. 16b), WASWind shows significant trends of decreasing wind during this season (red arrows in Fig. 16b).
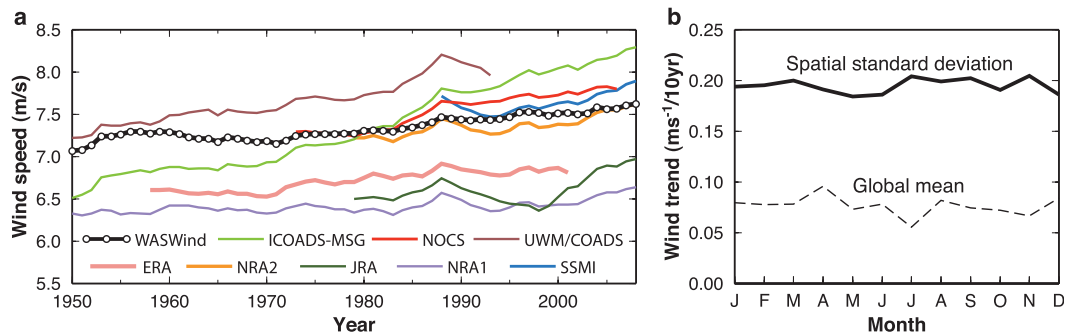
FIG. 14. (a) Time series of globally averaged annual scalar wind speed obtained from nine datasets. Each time series is smoothed with a 5-yr running average. (b) Spatial standard deviation of the scalar wind trend pattern (solid line in m s^{-1} decade^{-1}) and the trend of global-mean scalar wind speed (dashed line in m s^{-1} decade^{-1}) calculated from WASWind as a function of calendar month.

The trend of decreasing surface westerly winds is physically consistent with a relaxation of the meridional SLP gradient observed over the north Indian Ocean (Fig. 16c). ICOADS cloud cover has decreased over the Bay of Bengal and off the west coast of India for the period 1950–2008, consistent with the weakened circulation in WASWind and reduced Indian rainfall (Naidu et al. 2009).

5. Summary and discussion

We have constructed a new sea surface wind dataset, WASWind, from wind and wind wave observations archived in ICOADS ship reports. The dataset is available at monthly resolution for the period from 1950 to 2008 on a 4° × 4° latitude–longitude grid. To reduce the spurious upward trend in ship-observed surface wind, we have performed a series of wind adjustments and estimations as summarized below:

- anemometer-measured winds are adjusted with the height correction if HOA is available in ship metadata,
- visually estimated winds before (after) 1980 are adjusted with Lindau's equivalent wind scale (omitted),
- 10-m winds are estimated from visually observed wind wave heights by calibrating against height-corrected measured winds, and
- nighttime visual observations of wind and wave height are corrected with their averaged day − night difference.

As a result of these steps, WASWind represents well seasonal-to-decadal variability including the ENSO, IOD, PDO, and NAO. Most importantly, this dataset produces physically consistent long-term trends over the global oceans in comparison with independent satellite and SLP measurements. While the ICOADS HOA metadata and the height correction are available only after the late 1970s, our use of wave observations enables one to correct wind biases back to 1950. The extension of the corrected wind record helps improve trend pattern detection by suppressing natural variability.

WASWind is the first to estimate 10-m wind speed from visually observed wind wave heights in ICOADS. The advantage of using wave height observations is that they have been less affected by changes in observational practice than the sea surface wind (Gulev and Grigorieva 2004). The wind estimation from wave height is similar to

TABLE 3. Globally averaged scalar wind trends during six periods obtained from nine global datasets. Significant trends exceeding the 99% confidence level are emboldened, based on the Mann–Kendall test.

Dataset	Trend (m s^{-1} decade^{-1})					
	1950–2008	1950–93	1958–2001	1979–2008	1973–2006	1988–2008
ICOADS–MSG	**0.302**	**0.278**	**0.329**	**0.343**	**0.359**	**0.267**
WASWind	**0.074**	**0.057**	**0.079**	**0.107**	**0.104**	**0.084**
UWM–COADS	—	**0.193**	—	—	—	—
ERA	—	—	**0.081**	—	—	—
NRA2	—	—	—	**0.113**	—	**0.12**
JRA	—	—	—	0.102	—	0.171
NOCS v2.0	—	—	—	—	**0.197**	—
SSM/I	—	—	—	—	—	**0.134**
NRA1	**0.031**	**0.023**	0.016	**0.067**	**0.037**	**0.066**

a

SSM/I

b

WASWind

c

NOCS v2.0

-0.4 -0.3 -0.2 -0.1 0.0 0.1 0.2 0.3 0.4
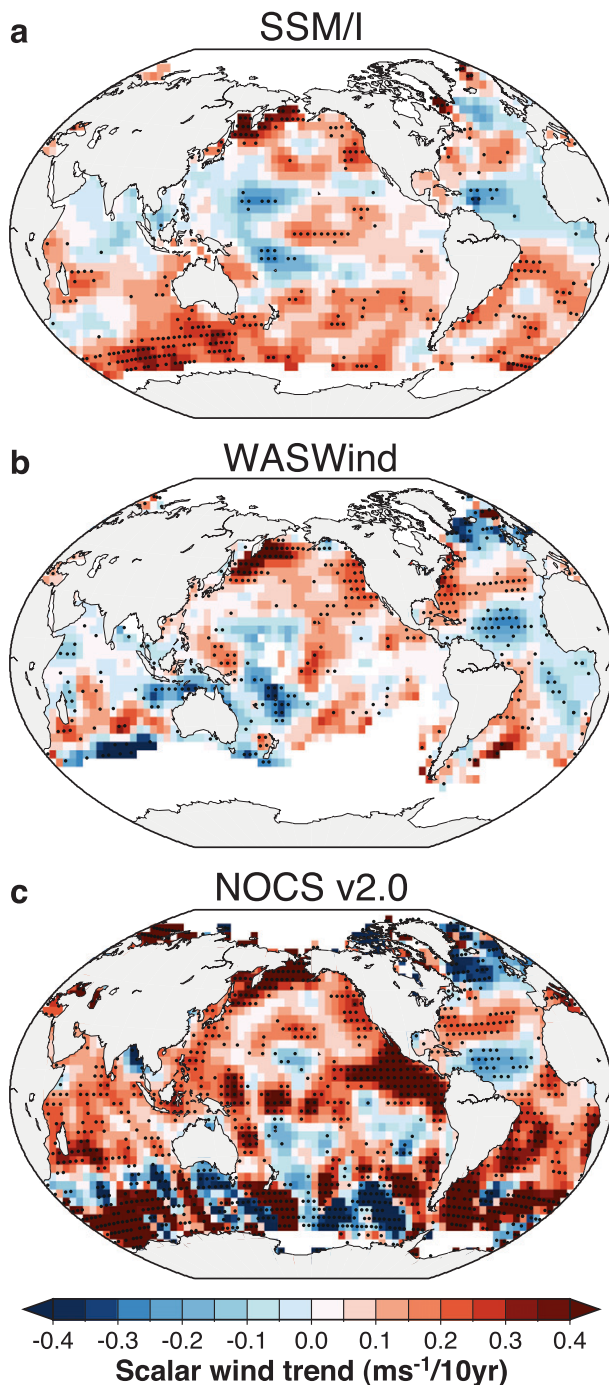**Scalar wind trend (ms⁻¹/10yr)**

FIG. 15. Linear trends in surface scalar-mean wind for the 20-yr period from July 1987 to August 2006 derived from (a) SSM/I, (b) WASWind, and (c) NOCS v2.0. Grid points marked with dots exceed the 95% confidence level based on the Mann–Kendall test.

TABLE 4. Comparison of WASWind and NOCS v2.0 scalar wind trends with the SSM/I for the period July 1987–August 2006. Bias is defined as WASWind (NOCS v2.0) minus SSM/I trends. The spatial correlation between WASWind (NOCS v2.0) and SSM/I exceeds the 95% (90%) confidence level. A two-tailed Student's t test is used for the significance test assuming that a degree of freedom is 15, estimated from numbers of regional patches showing positive and negative trends.

Dataset	Correlation	RMSD ($m\ s^{-1}\ decade^{-1}$)	Bias ($m\ s^{-1}\ decade^{-1}$)
WASWind	**0.50**	0.124	−0.011
NOCS v2.0	**0.44**	0.181	0.091

proportional to the square of surface wind speed (Fig. 6). There is a striking resemblance in the trend pattern between WASWind and SSM/I satellite wind data for the last two decades (Fig. 15). Moreover, WASWind reflects the long-term positive (negative) trend in wind wave height over the North Pacific (northeast Atlantic) during boreal winter revealed by Gulev and Grigorieva (2006). These findings suggest that WASWind is useful for climate trend analysis. While the Beaufort equivalent scale is a visual estimate of the sea surface wind from sea state, the estimated winds archived in ICOADS seem to be contaminated by anemometer-measured winds, especially after 1980, resulting in strong upward trends due to increases in both HOA and the ratio of measured to estimated winds (Cardone et al. 1990). While the measured wind can be adjusted to the 10-m height if HOA is available in the ship metadata, there is, unfortunately, no reliable correction method for the contaminated estimated winds.

Many previous studies have concluded that the upward wind trends for the last several decades are spurious (e.g., Isemer 1995; Ward and Hoskins 1996). Although the height correction effectively reduces ship-measured winds, a weak but significant upward trend still remains after the correction in most datasets. Some residual upward trends possibly result from other artificial factors such as a ship speed correction, flow distortion around anemometers (Blanc 1986; Moat et al. 2006a,b), and increased sampling of high-wind and rough-sea conditions by larger ships. Another possibility is that the residual upward trends may be real. For example, recent satellite observations by SSM/I exhibit a significant increasing trend in surface wind speed on the global average for the last 20 years (Wentz et al. 2007), and a similar increasing trend is found in WASWind and reanalysis products (Fig. 14a). Analyzing satellite observations for the period 1981–2006, Elsner et al. (2008) found an increase in maximum wind speed of the strongest tropical cyclones over the Atlantic and elsewhere, which may also contribute to the recent upward trend in sea surface wind.
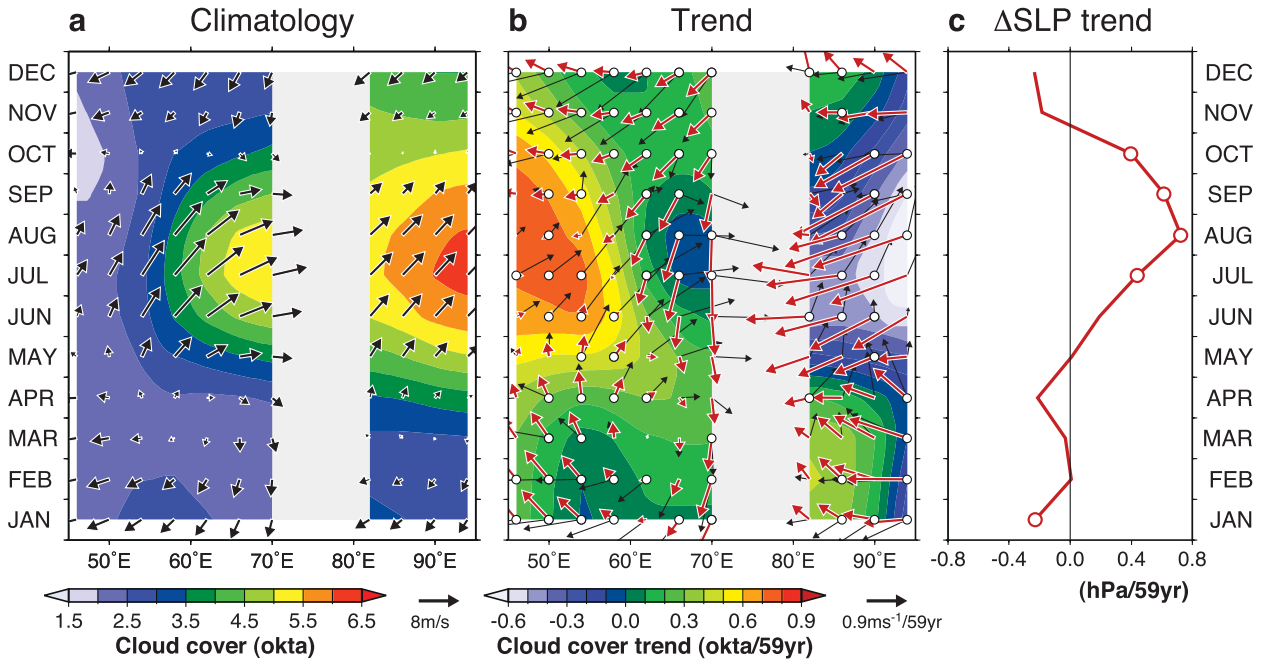
satellite measurements by microwave radiometers and scatterometers based on the assumption that the wind wave is generated by surface wind stress. Wind wave heights archived in ICOADS are found to be nearly

FIG. 16. ICOADS cloud cover and WASWind averaged over the north Indian Ocean (10°–20°N) as a function of longitude and calendar month: (a) Climatologies (color in okta for cloud cover, and vectors in m s^{-1} for surface wind) and (b) 59-year linear trends (color in okta for cloud cover, red vectors in m s^{-1} for WASWind, and black vectors for ICOADS unadjusted wind). (c) Monthly linear trend in meridional gradient of SLP defined as (12°–22°N) minus (2°–12°N) difference averaged between 62° and 94°E. Grid points marked with open circles exceed the 90% confidence level for trends in surface wind in (b) and meridional SLP gradient trend in (c).

While achieving a significant reduction of the upward trend, WASWind retains rich spatial patterns of the wind trend over the global oceans. The standard deviation of spatial variability is more than 2.5 times as large as the global-mean trend (Fig. 14b). For example, WASWind exhibits reductions in surface convergence over the Maritime Continent, the North Pacific trade winds, and the Indian summer monsoon (Figs. 11, 12, 13, and 16) that are physically consistent with BFF trends derived from the dynamical balance among the pressure gradient force, Coriolis force, and friction. WASWind appears to be a valuable dataset for studying patterns of wind change, which is an important element for other ocean and atmospheric changes such as those in sea level and precipitation.

WASWind successfully reproduces wind variabilities on seasonal-to-decadal and longer time scales, but some improvements are needed in the future. Our wind adjustments result in a considerable decrease in the total number of observations. We rejected anemometer-measured winds with unknown HOA and all visually estimated winds after 1980, and replaced them with wave height observations. Data-sparse regions, especially the Southern Ocean, can benefit from more observations. One possibility is to improve the availability of ship metadata. HOA contained in the ICOADS ship metadata is limited to about 50% of the total measured

wind reports for the recent three decades (Fig. 1a). The enhanced availability of HOA would increase reliable wind observations. The gridding method can also be improved. While a simple box average weighed by the number of observations was used in the present version of WASWind, more advanced objective analysis such as OI will be used for the next version to fill gaps and reflect the large-scale nature of wind variability. WASWind data are important for describing climate variability and trends and validating numerical model simulations, but further careful analysis will be required.

REFERENCES

Barnston, A. G., and R. E. Livezey, 1987: Classification, seasonality, and persistence of low-frequency atmospheric circulation patterns. *Mon. Wea. Rev.,* **115,** 1083–1126.

Berry, D. I., and E. C. Kent, 2009: A new air–sea interaction gridded dataset from ICOADS with uncertainty estimates. *Bull. Amer. Meteor. Soc.,* **90,** 645–656.

——, and ——, 2010: Air–sea fluxes from ICOADS: The construction of a new gridded dataset with uncertainty estimates. *Int. J. Climatol.,* doi:10.1002/joc.2059, in press.

Blanc, T. V., 1986: The effect of inaccuracies in weather-ship data on bulk-derived estimates of flux, stability, and sea surface roughness. *J. Atmos. Oceanic Technol.,* **3,** 12–26.

Bunker, A. F., 1980: Trends of variables and energy fluxes over the Atlantic Ocean from 1948 to 1972. *Mon. Wea. Rev.,* **108,** 720–732.

Cardone, V. J., J. G. Greenwood, and M. A. Cane, 1990: On trends in historical marine wind data. *J. Climate,* **3,** 113–127.

Clarke, A. J., and A. Lebedev, 1996: Long-term changes in the equatorial Pacific trade winds. *J. Climate,* **9,** 1020–1029.

da Silva, A. M., C. C. Young, and S. Levitus, 1994: *Atlas of Surface Marine Data 1994: Algorithms and Procedures.* Vol. 6, *World Ocean Atlas 1994,* NOAA Atlas NESDIS 6, 74 pp.

Deser, C., and M. L. Blackmon, 1993: Surface climate variations over the North Atlantic Ocean during winter: 1900–1989. *J. Climate,* **6,** 1743–1753.

——, and A. S. Phillips, 2006: Simulation of the 1976/77 climate transition over the North Pacific: Sensitivity to tropical forcing. *J. Climate,* **19,** 6170–6180.

——, and ——, 2009: Atmospheric circulation trends, 1950–2000: The relative roles of sea surface temperature forcing and direct atmospheric radiative forcing. *J. Climate,* **22,** 396–413.

——, ——, and J. W. Hurrell, 2004: Pacific interdecadal climate variability: Linkages between the tropics and the North Pacific during boreal winter since 1900. *J. Climate,* **17,** 3109–3124.

Du, Y., and S.-P. Xie, 2008: Role of atmospheric adjustments in the tropical Indian Ocean warming during the 20th century in climate models. *Geophys. Res. Lett.,* **35,** L08712, doi:10.1029/2008GL033631.

Elsner, J. B., J. P. Kossin, and T. H. Jagger, 2008: The increasing intensity of the strongest tropical cyclones. *Nature,* **455,** 92–95.

Fairall, C. W., E. F. Bradley, J. E. Hare, A. A. Grachev, and J. B. Edson, 2003: Bulk parameterization of air–sea fluxes: Updates and verification for the COARE algorithm. *J. Climate,* **16,** 571–591.

Gulev, S. K., and L. Hasse, 1999: Changes of wind waves in the North Atlantic over the last 30 years. *Int. J. Climatol.,* **19,** 1091–1117.

——, and V. Grigorieva, 2004: Last century changes in ocean wind wave height from global visual wave data. *Geophys. Res. Lett.,* **31,** L24302, doi:10.1029/2004GL021040.

——, and ——, 2006: Variability of the winter wind waves and swell in the North Atlantic and North Pacific as revealed by the voluntary observing ship data. *J. Climate,* **19,** 5667–5685.

Han, W., and Coauthors, 2010: Patterns of Indian Ocean sea-level change in a warming climate. *Nat. Geosci.,* **3,** 509–584.

Hanawa, K., S. Ishizaki, and Y. Tanimoto, 1996: Examination of the strengthening of wintertime mid-latitude westerlies over the North Pacific in the 1970s. *J. Meteor. Soc. Japan,* **74,** 715–721.

Hurrell, J. W., 1995: Decadal trends in the North Atlantic Oscillation: Regional temperatures and precipitation. *Science,* **269,** 676–679.

——, and H. VanLoon, 1997: Decadal variations in climate associated with the North Atlantic Oscillation. *Climatic Change,* **36,** 301–326.

Isemer, H.-J., 1995: Trends in marine surface winds speed: Ocean weather stations versus voluntary observing ships. *Proc. Int.*

COADS Workshop, Kiel, Germany, NOAA Environmental Research Laboratories and Institut für Meereskunde, 68–84.

——, and L. Hasse, 1991: The scientific Beaufort equivalent scale: Effects on wind statistics and climatological air–sea flux estimates in the North Atlantic Ocean. *J. Climate,* **4,** 819–836.

Kalnay, E., and Coauthors, 1996: The NCEP/NCAR 40-Year Reanalysis Project. *Bull. Amer. Meteor. Soc.,* **77,** 437–471.

Kanamitsu, M., W. Ebisuzaki, J. Woollen, S. K. Yang, J. J. Hnilo, M. Fiorino, and G. L. Potter, 2002: NCEP–DOE AMIP–II Reanalysis (R–2). *Bull. Amer. Meteor. Soc.,* **83,** 1631–1643.

Kent, E. C., and P. K. Taylor, 1997: Choice of a Beaufort equivalent scale. *J. Atmos. Oceanic Technol.,* **14,** 228–242.

——, S. D. Woodruff, and D. I. Berry, 2007: Metadata from WMO publication no. 47 and an assessment of voluntary observing ship observation heights in ICOADS. *J. Atmos. Oceanic Technol.,* **24,** 214–234.

Kutsuwada, K., 1994: On problems of ships-of-opportunity wind data on open ocean. *Umi Sora,* **14,** 49–53.

——, 2000: On problem of long-term surface wind variation using voluntary observing ship's data. *Proc. Int. Workshop on Preparation, Processing, and Use of Historical Marine Meteorological Data,* Tokyo, Japan, Japan Meteorological Agency and Ship and Ocean Foundation, 27–31.

Lindau, R., 1995: A new Beaufort equivalent scale. *Proc. Int. COADS Workshop,* Kiel, Germany, NOAA Environmental Research Laboratories and Institut für Meereskunde, 232–252.

Liu, W. T., X. S. Xie, and P. P. Niiler, 2007: Ocean–atmosphere interaction over Agulhas extension meanders. *J. Climate,* **20,** 5784–5797.

Mantua, N. J., S. R. Hare, Y. Zhang, J. M. Wallace, and R. C. Francis, 1997: A Pacific interdecadal climate oscillation with impacts on salmon production. *Bull. Amer. Meteor. Soc.,* **78,** 1069–1079.

Moat, B. I., M. J. Yelland, R. W. Pascal, and A. F. Molland, 2006a: Quantifying the airflow distortion over merchant ships. Part I: Validation of a CFD model. *J. Atmos. Oceanic Technol.,* **23,** 341–350.

——, ——, and A. F. Molland, 2006b: Quantifying the airflow distortion over merchant ships. Part II: Application of the model results. *J. Atmos. Oceanic Technol.,* **23,** 351–360.

Naidu, C. V., K. Durgalakshmi, K. M. Krishna, S. R. Rao, G. C. Satyanarayana, P. Lakshminarayana, and L. M. Rao, 2009: Is summer monsoon rainfall decreasing over India in the global warming era? *J. Geophys. Res.,* **114,** D24108, doi:10.1029/2008JD011288.

Nakamura, H., G. Lin, and T. Yamagata, 1997: Decadal climate variability in the North Pacific during the recent decades. *Bull. Amer. Meteor. Soc.,* **78,** 2215–2225.

Norris, J. R., 1998: Low cloud type over the ocean from surface observations. Part II: Geographical and seasonal variations. *J. Climate,* **11,** 383–403.

Onogi, K., and Coauthors, 2007: The JRA-25 Reanalysis. *J. Meteor. Soc. Japan,* **85,** 369–432.

Peterson, E. W., and L. Hasse, 1987: Did the Beaufort scale or the wind climate change? *J. Phys. Oceanogr.,* **17,** 1071–1074.

Ramage, C. R., 1987: Secular changes in reported surface wind speeds over the ocean. *J. Climate Appl. Meteor.,* **26,** 525–528.

Richter, I., and S. P. Xie, 2008: Muted precipitation increase in global warming simulations: A surface evaporation perspective. *J. Geophys. Res.,* **113,** D24118, doi:10.1029/2008JD010561.

Saji, N. H., B. N. Goswami, P. N. Vinayachandran, and T. Yamagata, 1999: A dipole mode in the tropical Indian Ocean. *Nature,* **401,** 360–363.

Smith, S. D., 1980: Wind stress and heat flux over the ocean in gale force winds. *J. Phys. Oceanogr.,* **10,** 709–726.

——, 1988: Coefficients for sea surface wind stress, heat flux, and wind profiles as a function of wind speed and temperature. *J. Geophys. Res.,* **93,** 15 467–15 472.

Smith, T. M., and R. W. Reynolds, 2003: Extended reconstruction of global sea surface temperatures based on COADS data (1854–1997). *J. Climate,* **16,** 1495–1510.

Tanimoto, Y., N. Iwasaka, K. Hanawa, and Y. Toba, 1993: Characteristic variations of sea surface temperature with multiple time scales in the North Pacific. *J. Climate,* **6,** 1153–1160.

Thomas, B. R., E. C. Kent, and V. R. Swail, 2005: Methods to homogenize wind speeds from ships and buoys. *Int. J. Climatol.,* **25,** 979–995.

——, ——, ——, and D. I. Berry, 2008: Trends in ship wind speeds adjusted for observation method and height. *Int. J. Climatol.,* **28,** 747–763.

Timmermann, A., S. McGregor, and F.-F. Jin, 2010: Wind effects on past and future regional sea level trends in the southern Indo-Pacific. *J. Climate,* **23,** 4429–4437.

Tokinaga, H., Y. Tanimoto, and S.-P. Xie, 2005: SST-induced surface wind variations over the Brazil–Malvinas confluence: Satellite and in situ observations. *J. Climate,* **18,** 3470–3482.

——, ——, ——, T. Sampe, H. Tomita, and H. Ichikawa, 2009: Ocean frontal effects on the vertical development of clouds over the western North Pacific: In situ and satellite observations. *J. Climate,* **22,** 4241–4260.

Trenary, L. L., and W. Han, 2008: Causes of decadal subsurface cooling in the tropical Indian Ocean during 1961–2000. *Geophys. Res. Lett.,* **35,** L17602, doi:10.1029/2008GL034687.

Uppala, S. M., and Coauthors, 2005: The ERA-40 Re-Analysis. *Quart. J. Roy. Meteor. Soc.,* **131,** 2961–3012.

Vecchi, G. A., B. J. Soden, A. T. Wittenberg, I. M. Held, A. Leetmaa, and M. J. Harrison, 2006: Weakening of tropical Pacific atmospheric circulation due to anthropogenic forcing. *Nature,* **441,** 73–76.

Wallace, J. M., E. M. Rasmusson, T. P. Mitchell, V. E. Kousky, E. S. Sarachik, and H. von Storch, 1998: The structure and evolution of ENSO-related climate variability in the tropical Pacific: Lessons from TOGA. *J. Geophys. Res.,* **103,** 14 241–14 259.

Ward, M. N., and B. J. Hoskins, 1996: Near-surface wind over the Global Ocean 1949–1988. *J. Climate,* **9,** 1877–1895.

Webster, P. J., A. M. Moore, J. P. Loschnigg, and R. R. Leben, 1999: Coupled ocean–atmosphere dynamics in the Indian Ocean during 1997–98. *Nature,* **401,** 356–360.

Wentz, F. J., 1997: A well-calibrated ocean algorithm for special sensor microwave/imager. *J. Geophys. Res.,* **102,** 8703–8718.

——, L. Ricciardulli, K. Hilburn, and C. Mears, 2007: How much more rain will global warming bring? *Science,* **317,** 233–235.

Whysall, K. D. B., N. S. Cooper, and G. R. Bigg, 1987: Long-term changes in the tropical Pacific surface wind field. *Nature,* **327,** 216–219.

Woodruff, S. D., R. J. Slutz, R. L. Jenne, and P. M. Steurer, 1987: A comprehensive ocean–atmosphere data set. *Bull. Amer. Meteor. Soc.,* **68,** 1239–1250.

——, and Coauthors, 2010: ICOADS release 2.5: Extensions and enhancements to the surface marine meteorological archive. *Int. J. Climatol.,* doi:10.1002/joc.2103, in press.

Worley, S. J., S. D. Woodruff, R. W. Reynolds, S. J. Lubker, and N. Lott, 2005: ICOADS release 2.1 data and products. *Int. J. Climatol.,* **25,** 823–842.

Wu, B. Y., 2005: Weakening of Indian summer monsoon in recent decades. *Adv. Atmos. Sci.,* **22,** 21–29.

Wu, R., and S.-P. Xie, 2003: On equatorial Pacific surface wind changes around 1977: NCEP–NCAR reanalysis versus COADS observations. *J. Climate,* **16,** 167–173.

Xie, S.-P., and S. G. H. Philander, 1994: A coupled ocean–atmosphere model of relevance to the ITCZ in the eastern Pacific. *Tellus,* **46A,** 340–350.

——, C. Deser, G. A. Vecchi, J. Ma, H. Teng, and A. T. Wittenberg, 2010a: Global warming pattern formation: Sea surface temperature and rainfall. *J. Climate,* **23,** 966–986.

——, Y. Du, G. Huang, X. T. Zheng, H. Tokinaga, K. M. Hu, and Q. Y. Liu, 2010b: Decadal shift in El Niño influences on Indo–western Pacific and East Asian climate in the 1970s. *J. Climate,* **23,** 3352–3368.

Zebiak, S. E., 1993: Air–sea interaction in the equatorial Atlantic region. *J. Climate,* **6,** 1567–1568.

Zheng, X. T., S.-P. Xie, G. A. Vecchi, Q. Y. Liu, and J. Hafner, 2010: Indian Ocean dipole response to global warming: Analysis of ocean–atmospheric feedbacks in a coupled model. *J. Climate,* **23,** 1240–1253.